ELSEVIER

Journal of Photochemistry and Photobiology A: Chemistry 150 (2002) 213–221

Journal of Photochemistry and Photobiology A:Chemistry

www.elsevier.com/locate/jphotochem

EPR study of the radicals formed upon UV irradiation of ceria-based photocatalysts

Juan M. Coronado*, A. Javier Maira, Arturo Martínez-Arias, José Carlos Conesa, Javier Soria

Instituto de Catálisis y Petroleoquímica, CSIC, Campus Cantoblanco, 28049 Madrid, Spain

Received 6 February 2002; accepted 12 February 2002

Abstract

EPR measurements reveal remarkable differences on the type of radicals produced after UV illumination of TiO_2, CeO_2 and 0.8% CeO_2/TiO_2 photocatalysts. Photoactivation of the TiO_2 sample in vacuum results in the formation of Ti^{4+}–O^- species and a small amount of Ti^{3+} centers. In the presence of adsorbed oxygen, irradiation of this material also generates Ti^{4+}–O_3^- radicals. In the case of the CeO_2/TiO_2 catalyst, the ceria component is present in a highly dispersed state, as indicated by XRD and UV–Vis diffuse reflectance spectra (DRS) results. Accordingly, the only type of Ce^{4+}–O_2^- adducts generated on the CeO_2/TiO_2 sample are indicative of the presence of two-dimensional patches of ceria on the anatase surface. On the other hand, photoactivation of the CeO_2/TiO_2 sample in the presence of oxygen also leads to the formation of some Ti^{4+}–O^- and Ti^{3+} centers. In the case of the CeO_2 sample, superoxide radicals are observed upon irradiation in vacuum and subsequent oxygen adsorption. Further irradiation of this material in the presence of oxygen increases the amount of Ce^{4+}–O_2^- radicals and simultaneously generates new species, which are tentatively assigned to Ce^{4+}–O_2H radicals. Photocatalytic activity was tested for toluene oxidation, and the results obtained show that the photodegradation rate is slightly lower for CeO_2/TiO_2 than for the TiO_2 sample. However, the selectivity towards benzaldehyde (6–13%) is comparable for both materials. In the case of CeO_2, the photo-oxidation rate is an order of magnitude lower than for TiO_2, although mineralization of toluene is almost complete. Photoactivity results are discussed in connection with the characteristics of the radicals observed.

Keywords: Photocatalysis; EPR; Cerium oxide; Titanium oxide; Oxygen radicals

1. Introduction

Volatile organic compounds (VOCs) are widespread pollutants originated by either industrial or domestic sources [1]. Many of them are known to be noxious and/or carcinogenic and consequently there is a considerable concern about the consequences of exposing the population to these substances. In order to limit these risks for the health, several methods for the removal of these compounds have been proposed. Among them, photocatalytic oxidation (PCO) constitutes a promising alternative because of its capability of mineralizing a variety of chemicals under mild conditions [2,3]. Nevertheless, the most active photocatalyst, the anatase form of TiO_2, presents a moderate quantum yield and the total oxidation of certain substrates is not easily achieved. Formation of a substantial amount of partially oxidized products is another issue that has to be addressed when removing certain pollutants, like toluene and xylene [4]. In addition, partial deactivation of the catalyst is occasionally observed, especially when photo-oxidizing aromatic substrates [4,5]. In order to overcome these difficulties, several modifications of the photocatalysts have been proposed. Careful control of the nanoscale structure of the TiO_2 samples leads to a considerable improvement of their PCO performance [6,7]. Incorporation of noble metals like platinum to the photocatalysts can also result in an increase of the mineralization rate, most likely due to the stabilization of the photoproduced charge carriers [8]. In a similar way, insertion of transition metal ions on the titania structure can significantly enhance the photonic efficiency, either by widening the light absorption range or by modifying the redox potential of the photoproduced radicals [3,9,10]. An alternative approach is establishing electronic contacts between different semiconductors [3,11]. In such case, a suitable choice of the materials brought into contact can enhance the photocatalytic activity by increasing the efficiency for charge separation [11].

CeO_2 is frequently incorporated to the formulation of oxidation catalysts because it shows a considerable performance for the catalytic combustion of hydrocarbons and CO [12]. The formation/annihilation of oxygen vacancies in redox processes occurring on the surface of ceria-containing samples is considered to play a crucial role on these oxidative reactions [12]. On the other hand, ceria is an n-type

* Corresponding author. Fax: +34-91-5854760.
E-mail address: jmcoronado@icp.csic.es (J.M. Coronado).

1010-6030/02/$ – see front matter
PII: S1010-6030(02)00092-8

semiconductor with a bandgap of 2.94 eV, and consequently it can be photoactivated by irradiation with light in the near-UV–Vis range [13]. These characteristics suggest that CeO_2 could be potentially used as a photocatalyst for the oxidation of pollutants. However, there are only a few reports on the photoactivity in aqueous solutions of materials containing cerium oxide [13,14], and consequently additional studies are desirable.

The EPR spectroscopy is an especially suitable technique for the detection of photogenerated radicals, which act as intermediates in the photocatalytic processes [3]. Formation of trapped-hole centers upon UV irradiation has been observed in the bulk of CeO_2 single crystals by means of this technique [15]. However, to our knowledge, there are no reports about the UV-induced formation of surface radicals on ceria-based powder catalysts. In this work, the TiO_2, CeO_2/TiO_2 and CeO_2 samples are studied by means of EPR spectroscopy following near-UV irradiation, in an attempt to establish the mechanism of the transference of the photogenerated charge carriers to the surface or between phases. In addition, in order to assess the possible application of these materials to decontamination processes, their photocatalytic activity for the mineralization of toluene vapor, which is a prevalent VOC [1], was also tested at moderate temperatures (343–413 K). The results obtained have been analyzed in connection with the characteristics of the photogenerated radicals detected by EPR.

2. Experimental details

2.1. Materials

Commercial TiO_2 (supplied by BDH; purity > 98%; $S_{BET} = 10\,m^2\,g^{-1}$) and CeO_2 (Rhône-Poulenc, $S_{BET} = 109\,m^2\,g^{-1}$) samples were used without further treatment. The CeO_2/TiO_2 sample, referred to as CeTi, was prepared by incipient wetness impregnation of the titania support with an aqueous solution of $Ce(NO_3)_3{\cdot}6H_2O$ (Aldrich), in order to obtain a final ceria loading of 0.80 wt.% (corresponding to 25% of the theoretical monolayer). After overnight drying at 383 K, the resulting powder was calcined in air at 773 K for 2 h, increasing the temperature from room temperature (RT) at a rate of $2\,K\,min^{-1}$. These materials were stored in air before their use.

2.2. Techniques

BET surface areas were measured at 77 K after overnight outgassing treatment at 423 K, using a Micromeritics equipment. XRD experiments were carried out in a Seifert apparatus employing nickel-filtered Cu Kα radiation. UV–Vis diffuse reflectance experiments were performed with a Shimadzu UV2100 spectrometer equipped with an integrating sphere and using powdered $Ba(SO_4)_2$ as a reference. FTIR spectra were recorded by accumulation of 200 scans with a resolution of $4\,cm^{-1}$ in a Nicolet 5 ZDX equipment provided with an MCT detector, using self-supported discs ($\approx 35\,mg\,cm^{-2}$).

EPR measurements were carried out at 77 K with a Bruker ER200D spectrometer operating in the X-band and using DPPH ($g = 2.0036$) for frequency calibration. Computer simulations were used when necessary to check spectral parameters. Quantitative analyses were carried out by double integration of the spectra and comparison with a $Cu(SO_4){\cdot}5H_2O$ standard. Aliquots of the catalyst (30–40 mg) were placed into a quartz probe cell with greaseless stopcocks, which can be externally heated with a tubular furnace. Outgassing treatments were carried out for 1 h using a conventional high vacuum line, which is able to achieve dynamic pressures lower than $2 \times 10^{-2}\,N\,m^2$. For adsorption experiments, a fixed dose ($\approx 100\,\mu mol$ per gram of sample) of oxygen (SEO; purity = 99.9%, further purified by several freeze-pump-thaw cycles) was admitted in the cell at 77 K, and subsequently outgassed at the same temperature in order to remove weakly adsorbed (physisorbed) oxygen. Irradiation treatments were performed ex situ by placing the cell during 15 min in a quartz Dewar flask at 77 K and using three fluorescent lamps (Osram *Eversun* L40 W/79 K, maximum intensity at 350 nm) as UV source.

2.3. Photocatalytic activity tests

An annular photoreactor constituted of two concentric tubes of Pyrex, externally illuminated by four fluorescent lamps of black light (Sylvania, 6WBLB-T5, 6 W, maximum at 365 nm) was used for these measurements. The gas mixture flows through the space between the two glass cylinders. A slurry of catalyst powder in ethanol was spread on the external surface of the inner glass cylinder. After drying at room temperature for 1 day, the catalyst forms a relatively uniform coating over the reactor surface. Temperatures in the 343–413 K range were obtained by means of a heater wire controlled with a thermocouple, both placed in the center of the inner tube of the photoreactor. Toluene (Aldrich, HPLC grade) was introduced into the stream of humid oxygen (100 sccm; ca. 75% relative humidity) by means of a syringe pump (kdScientific 1000) at the rate appropriate for achieving a constant concentration of 1200 ppmv. Analysis of the outlet flow was carried out by means of a Hewlett Packard G1800 MS-GC, using a capillary column of medium polarity ($0.32\,mm \times 30\,m$) and the SIM mode of the detector. Further details of the experimental set-up can be found elsewhere [7].

3. Results and discussion

3.1. Characterization of the catalysts

Both XRD and BET area measurements indicate that the textural and bulk structural properties of the TiO_2 are not

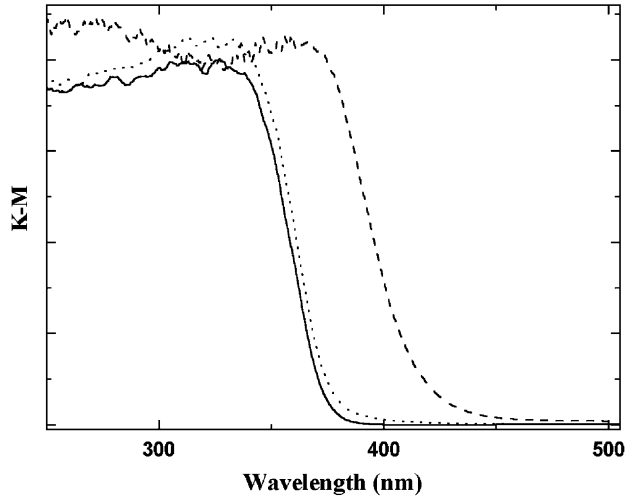

Fig. 1. UV–Vis DRS of the TiO_2 (solid line), CeO_2/TiO_2 (dotted line) and CeO_2 (dashed line).

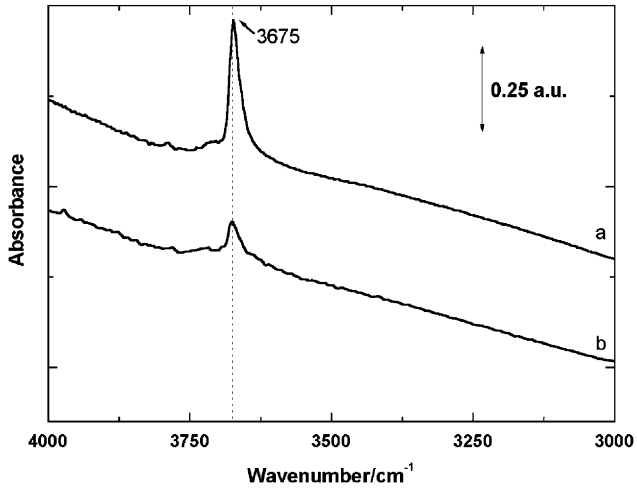

Fig. 2. FTIR spectra of (a) TiO_2 and (b) CeO_2/TiO_2 catalysts outgassed at 423 K for 1 h.

significantly modified upon ceria addition. Thus, the specific surface of the CeTi sample, 11 $m^2\,g^{-1}$, is comparable to that of the pure TiO_2 sample (10 $m^2\,g^{-1}$). XRD patterns for both samples are similar, and they present exclusively reflections of the anatase phase. These results suggest that a well-dispersed state of the ceria component is achieved, and no apparent modification of the TiO_2 is produced. The XRD pattern of the CeO_2 sample corresponds to the fluorite structure characteristic of this compound.

UV–Vis diffuse reflectance spectra (DRS) of the samples are plotted in Fig. 1. Although the CeO_2 sample presents its absorption edge at ca. 370 nm, the spectrum of CeTi shows that ceria incorporation to TiO_2 induces only a small red shift of the electronic absorption with respect to the pure anatase. Previous studies on supported ceria samples have shown an increasing blue shift of the absorption edge of this material with decreasing the ceria loading and, consequently the ceria average particle size [16–18]. This fact has been proposed to arise as a consequence of either the quantum size effect originated by the diminution of ceria particle size, or the existence of larger contribution of Ce^{4+}–O^{2-} charge transfer transitions, which yields a relatively broad band with a maximum at ca. 380 nm [16]. Accordingly, small ceria particles, or highly dispersed cerium entities (either isolated or forming two-dimensional ceria patches on the support surface) display a larger intensity of the charge transfer transition than the corresponding bulk oxide [16,17]. On this basis, the modification of the spectrum of CeTi with respect to TiO_2 is consistent with the presence of a dispersed ceria component (in the form of very small crystallites or as highly dispersed two-dimensional entities) superimposed on the spectrum of the TiO_2 support.

Fig. 2 displays the FTIR spectra of the CeTi/TiO_2 and TiO_2 samples in the 4000–3000 cm^{-1} range after outgassing at 423 K for 1 h. Following this treatment, broad features in the O–H stretching range are entirely removed and only a sharp band remains at 3765 cm^{-1}. This feature appears in the spectra of both samples and corresponds to isolated OH groups at the surface [19]. The lower intensity of this band for the CeTi catalysts indicates that CeO_2 incorporation partly depletes the TiO_2 surface of hydroxyl groups.

3.2. EPR study of the samples thermally activated in vacuum

The EPR spectra obtained after room temperature (RT) evacuation for 1 h of the TiO_2 and CeTi samples (not shown) consist of a set of sharp features at $g = 2.004$, 1.989, 1.971 and 1.945, which does not correspond to any of the species usually found on TiO_2 samples. They are very likely related to cationic impurities of the anatase. A feasible assignment is substitutional Cr^{3+} in the TiO_2 lattice, which gives rise to similar features, attributed to transitions within a triplet state ($S = \frac{3}{2}$) [21]. Anyhow, the influence of these foreign ions on the photocatalytic activity must be quite limited since the performance of this catalyst is similar to that of other commercial TiO_2 samples (see below). In addition, except for minor changes in the linewidth, these features remain basically unchanged after the treatments performed in the present study. Therefore, for the sake of clarity, these background contributions have been subtracted to the spectra shown hereafter.

Fig. 3 displays the EPR spectra of the CeO_2, CeO_2/TiO_2 and TiO_2 catalysts submitted to thermal treatments in vacuum at different temperatures and subsequently contacted with oxygen. When oxygen is adsorbed at RT on the CeO_2 sample previously outgassed at 473 K, the spectrum obtained (Fig. 3a) is constituted by signal OC1, with parameters $g_{\parallel} = 2.037$ and $g_{\perp} = 2.011$. This signal is characteristic of superoxide radicals adsorbed on cerium cations, which in contrast with the predictions of the ionic model followed by most of these species, does not present any g-component close to g_e

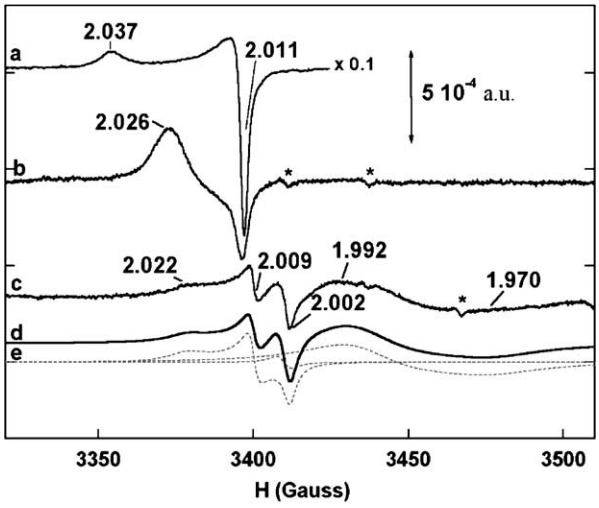

Fig. 3. EPR spectra of (a) CeO_2 outgassed at 473 K and exposed to oxygen at RT; (b) the CeO_2/TiO_2 catalyst outgassed at 373 K for 1 h and contacted with O_2 at 77 K; (c) TiO_2 sample outgassed at 673 K for 1 h and contacted with O_2 at 77 K; (d) computer simulation of the previous spectrum; (e) spectrum deconvolution into single components. Background contributions of the TiO_2 and CeTi materials obtained prior to O_2 adsorption have been subtracted. The asterisk marks features result from the incomplete cancellation of those background signals.

(i.e. free electron value, $g_e = 2.0023$) [18,20,22]. This fact has been related to the participation of 4f orbitals in the bond [18,20,22], and allows distinguishing these species from the corresponding radicals adsorbed on titanium ions [7,23]. Considering that ceria-containing materials are slightly reduced under thermal treatment in vacuum, oxygen vacancies and Ce^{3+} centers are very likely involved on superoxide formation [18,20], following a process that can be envisaged as (using formal charges) $Ce^{3+}–V_{Ö} + O_2 \rightarrow Ce^{4+}–O_2^-$. It must be noted here that EPR detection of paramagnetic $Ce^{3+}–V_{Ö}$ centers in the present experimental conditions is hindered by the low spin relaxation time of such species [18]. On the other hand, if the outgassing temperature is higher than 673 K, new signals are detected, which have been related to superoxide species formed on associated vacancies centers on the ceria surface, in contrast with the isolated vacancies required to generate signal OC1 [18,20].

In the case of sample CeTi treated in vacuum at 373 K and exposed to oxygen at 77 K (Fig. 3b), the EPR spectrum exclusively shows, after removing the background contribution, signal OC2 with parameters $g_z = 2.026$, $g_x = 2.018$ and $g_y = 2.011$ (axes assignment according to previous reports [18,22]). This signal is also observed, although with lower intensity following RT outgassing and subsequent oxygen adsorption (not shown). Signals with the g_x-parameter shifted to lower field with respect to the signals observed for unsupported ceria (i.e. OC1 for which $g_{x,y} = g_\perp = 2.011$) have been observed when studying ceria dispersed on different carrier oxides [18,20,22]. They have been assigned to $Ce^{4+}–O_2^-$ adducts with larger covalent character than the equivalent species formed on the bulk oxide [18,20,22]. These radicals, as those generating signal OC2, are highly labile, and they rapidly disappear following RT outgassing due to O_2 desorption [18,20]. According to these arguments, formation of $Ce^{4+}–O_2^-$ species on CeTi indicates that vacuum treatments generate, even at RT, reduced cerium cations with doubly ionized oxygen vacancies in their coordination sphere ($Ce^{3+}–V_{Ö}$ centers). Double integration of the spectra of the CeTi sample outgassed at $T_v = 373$ and 773 K, and subsequently contacted with oxygen at 77 K, indicate that the amount of superoxide radicals present correspond, respectively, to the 0.02 and the 6% of the total cerium content. Considering their relatively large g_x-value and instability towards RT outgassing, the entities giving rise to signal OC2 must correspond to two-dimensional ceria patches (2D-Ce) [18,20]. Therefore, resuming the discussion on DRS UV–Vis results, the dispersed ceria entities in CeTi should be envisaged as forming 2D-Ce entities rather than small ceria particles.

In the case of pure TiO_2, new signals are generated after oxygen adsorption on samples previously outgassed at $573\,K \leq T_v \leq 773\,K$. Fig. 3c displays the results obtained after exposing the anatase sample pretreated in vacuum at $T_v = 673$ K to oxygen at 77 K. Computer simulation (Fig. 3d) shows that this spectrum consists of three components (Fig. 3e): signal OT1 with $g_1 = 2.022$, $g_2 = 2.009$ and $g_3 = 2.002$; signal D with $g = 2.003$; and signal T with $g_\perp = 1.988$ and $g_\parallel = 1.965$. According to previous studies, signal OT1 corresponds to $Ti^{4+}–O_2^-$ adducts on the anatase surface [23]. Species of the type T can be related to Ti^{3+} centers formed by thermal treatment in vacuum of the TiO_2 [23]. Although reduced titanium ions in anatase usually give rise to sharper features, as expected for isolated cations in a homogeneous environment, the values of the g-tensor of signal T are similar to those previously reported for Ti^{3+} centers in the bulk of TiO_2 ($g_\perp = 1.992$–88 and $g_\parallel = 1.962$–60) [23,24]. In accordance with this, signal T is not modified in the presence of oxygen, and consequently can be ascribed to Ti^{3+} sites in the bulk. Considering the high crystallinity of the TiO_2 used in the present study, the relatively large width of signal T could be due to by magnetic interactions with foreign cations (i.e. Cr^{3+}). Finally, the symmetric feature D can be assigned to electrons trapped in anionic vacancies at the TiO_2 lattice [23]. On the other hand, it is worth noting that when the CeTi sample is treated in the same conditions no signal attributable to $Ti^{4+}–O_2^-$ species is detected, but only OC2 radicals are observed. This fact suggests that CeO_2 addition modifies the sites where OT1 surface complexes are attached.

3.3. EPR study of photogenerated radicals

In order to obtain information about the photo-induced processes occurring in these samples, the catalysts were irradiated at 77 K, either under vacuum or in the presence of pre-adsorbed O_2. The components of the g-tensor and the

Table 1
EPR parameters and assignment of photogenerated radicals detected on TiO_2, CeO_2/TiO_2 and CeO_2 samples

Signal	EPR parameters	Proposed assignment
OT1	$g_1 = 2.022$; $g_2 = 2.009$; $g_3 = 2.002$	Ti^{4+}–O_2^-
OT2	$g_1 = 2.025$; $g_2 = 2.015$; $g_3 = 2.003$	Ti^{4+}–O^-
OT3	$g_1 = 2.009$; $g_2 = 2.005$; $g_3 = 2.002$	Ti^{4+}–O_3^-
OC1	$g_\parallel = 2.037$; $g_\perp = 2.011$	Ce^{4+}–O_2^- on bulk CeO_2
	$g_1 = 2.033$; $g_2 = 2.012$; $g_3 = 2.011$	
OC2	$g_z = 2.026$–5; $g_y = 2.018$; $g_x = 2.011$	Ce^{4+}–O_2^- on 2D patches
OC3	$g_1 = 2.036$; $g_2 = 2.012$; $g_3 = 2.002$	Ce^{4+}–O_2H
T	$g_\perp = 1.988$; $g_\parallel = 1.965$	Ti^{3+} in the bulk

assignments proposed for the EPR signals detected under these conditions are summarized in Table 1. Fig. 4 shows the EPR spectra obtained in these experiments for the TiO_2 sample upon photoactivation. Following RT outgassing for 1 h and subsequent UV illumination at 77 K (Fig. 4a) signal OT2 is observed, whose parameters obtained by computer simulation are $g_1 = 2.025$, $g_2 = 2.015$ and $g_3 = 2.003$. Previous studies on different TiO_2 samples exposed to UV

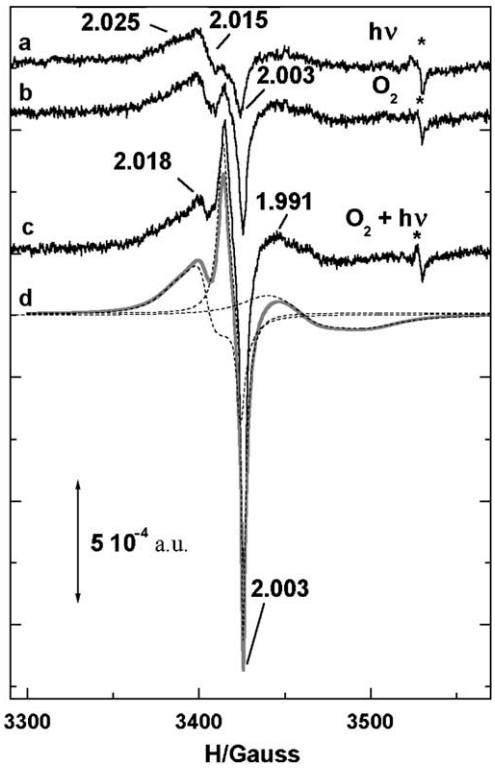

Fig. 4. EPR spectra of the TiO_2 sample outgassed at RT for 1 h: (a) UV irradiated for 15 min; (b) subsequently contacted with O_2 at 77 K; (c) finally irradiated for 15 min at 77 K. The background spectrum obtained after evacuation at RT has been subtracted; asterisk marks denote incomplete cancellation of background signals. (d) Computer simulation (thick line) with the corresponding deconvolution into single components (dashed line) of the spectrum (c).

light revealed the formation of signals similar to OT2 that have been assigned to Ti^{4+}–O^- species [24–26]. Thus, Micic et al. [25] observed a relatively broad spectrum displaying extrema at $g = 2.018$ and $g = 2.004$ upon irradiation of colloidal TiO_2. These authors ascribed this signal to surface Ti^{4+}–O^- radicals and reported the following parameters: $g_x = 2.007$, $g_y = 2.014$ and $g_z = 2.024$. More recently, Nakaoka and Nosaka [26] detected on different TiO_2 samples two distinct signals associated to hole-trapped species: subsurface entities Ti^{4+}–O^-–Ti^{4+}–OH^-, with $g_1 = 2.004$, $g_2 = 2.014$ and $g_3 = 2.018$; and surface radicals Ti^{4+}–O^{2-}–Ti^{4+}–O^-, with $g_1 = 2.004$, $g_2 = 2.018$ and $g_3 = 2.030$. On this basis, signal OT2 is assigned to Ti^{4+}–O^- species, which, according to its parameters and behavior (see below), are very likely located at surface sites. The presence of Ti^{3+} centers is not evident in the spectrum of Fig. 4a, but T-type signals are clearly observed after irradiation in the presence of oxygen (Fig. 4c). Therefore, following the generally accepted mechanism, TiO_2 photoactivation can be considered to take place according to

$$TiO_2 + h\nu \rightarrow TiO_2\,(h^+ + e^-) \quad (1)$$

$$h^+ + Ti^{4+}\text{–}O^{2-} \rightarrow Ti^{4+}\text{–}O^- \quad (2)$$

$$e^- + Ti^{4+} \rightarrow Ti^{3+} \quad (3)$$

Subsequent oxygen adsorption at 77 K on the previously irradiated TiO_2 (Fig. 4b) leads to the formation of a new signal, OT3, with components at $g_1 = 2.009$, $g_2 = 2.005$ and $g_3 = 2.002$ (Fig. 4d). This feature can be ascribed to O_3^- radicals [26] formed according to

$$Ti^{4+}\text{–}O^- + O_2 \rightarrow Ti^{4+}\text{–}O_3^- \quad (4)$$

Subsequent irradiation at 77 K in the presence of oxygen (Fig. 4c) results in a considerable rise of the concentration of OT3 species, along with a moderate increment of the amplitude of OT2 signals. As mentioned above, the amount of Ti^{3+} also increases under these conditions (Fig. 4c).

Fig. 5 displays the EPR results obtained for CeTi submitted to the same treatments. Following irradiation in vacuum at 77 K (Fig. 5a), a poorly resolved signal with features at $g = 2.009$ and $g = 2.003$, along with a certain amount of signal T is detected. Although the exact parameters of the g-tensor of the former signal are difficult to ascertain due to their reduced amplitude, it must correspond to some kind of oxygenated radicals on titanium centers, since all these species share a component at ca. $g = 2.003$ (i.e. signals OT1 and OT2) [24–27]. The spectrum obtained after oxygen adsorption at 77 K on the sample previously irradiated (Fig. 5b) shows the formation of OC2 radicals, whereas the other signals present prior to O_2 adsorption do not significantly change. Considering that RT outgassing and subsequent oxygen adsorption results in the generation of a lower amount of Ce^{4+}–O_2^- radicals, it can be concluded that previous UV irradiation assists to the formation of OC2 species. In addition, the intensity of the OC2 signal slightly

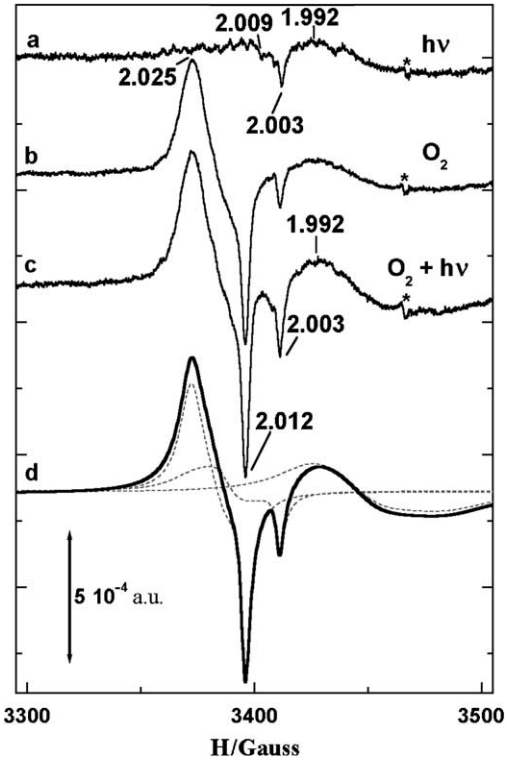

Fig. 5. EPR spectra of the CeTi sample outgassed at RT for 1 h: (a) UV irradiated for 15 min; (b) subsequently contacted with O_2 at 77 K; (c) finally irradiated for 15 min at 77 K. The background spectrum obtained after evacuation at RT has been subtracted; asterisk marks denote incomplete cancellation of background signals. (d) Computer simulation (thick line) with the corresponding deconvolution into single components (dashed line) of the spectrum (c).

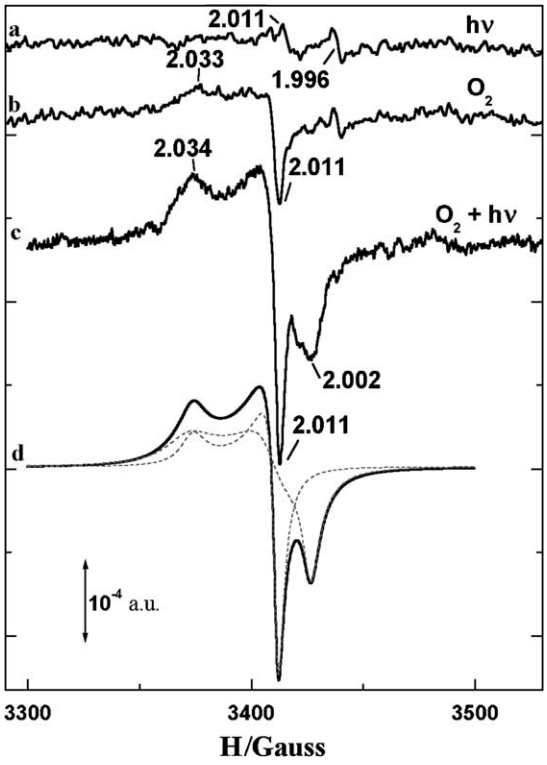

Fig. 6. EPR spectra of the CeO_2 sample outgassed at RT for 1 h: (a) UV irradiated for 15 min; (b) subsequently contacted with O_2 at 77 K; (c) finally irradiated for 15 min at 77 K; (d) Computer simulation (thick line) with the corresponding deconvolution into single components (dashed line) of the spectrum (c).

increases by UV illumination at 77 K in the presence of oxygen (Fig. 5c). Computer simulation shows (Fig. 5d) that following this treatment the amount of radicals located at the TiO_2 component of the CeTi sample (corresponding to signals T and OT2) also increases. It must be noted that the amount of photogenerated holes stabilized as Ti^{4+}–O^- radicals upon irradiation in vacuum of the CeTi material is lower than for the TiO_2 sample, although similar amounts of these species are generated in the presence of oxygen (Figs. 4d and 5d).

The results of parallel experiments performed on the CeO_2 sample are shown in Fig. 6. Irradiation of this material under vacuum at 77 K gives rise to very weak signals showing ill-defined features at $g = 1.996$ and 2.012 (Fig. 6a), which could arise from photoproduced charge carriers trapped at defects and/or impurities of the solid. Subsequent oxygen adsorption at 77 K produces a signal, OC1′, with $g_z = 2.033$, $g_x = 2.012$ and $g_y = 2.011$ (Fig. 6b), which is characteristic of Ce^{4+}–O_2^- complexes at the surface of partially hydroxylated CeO_2 [18,20]. The spectrum recorded after irradiation of ceria at 77 K in the presence of O_2 (Fig. 6c) presents two main contributions, as indicated by computer simulation: OC1′, and OC3, broader and with components at $g_1 = 2.036$, $g_2 = 2.012$ and $g_3 = 2.002$ (Fig. 6d). Signal OC3 presents one of its g-components rather close to g_e, a characteristic that, as mentioned above, differs from those of O_2^- radicals detected on ceria-containing materials [18,20,22]. Previous studies showed that UV irradiation of pure CeO_2 single crystals at 77 K produces several related signals with g-components reported in the following ranges: $g_x = 2.031$–18, $g_y = 2.005$–7 and $g_z = 2.041$–32 [15]. These signals have been attributed to O_2^{3-} (O^-–O^{2-}) radicals, formed by trapping of a photogenerated hole between two oxide anions [15], although the existence of such diatomic radicals has been questioned due to the lack of studies with ^{17}O [28]. Nevertheless, the g-parameters of OC3 signal are closer to those found experimentally and theoretically for O_2H molecules: $g_1 = 2.035$, $g_2 = 2.009$ and $g_3 = 2.003$ [29]. These species are formed by protonation of superoxide radicals, and they are frequently detected upon UV irradiation of hydrated TiO_2 [3,7]. Consistently, signal OC3 is also related to the presence of surface water/hydroxyls groups because it is not generated if the CeO_2 sample is outgassed at high temperature previously to irradiation. Therefore, although additional studies are required to confirm the assignment, OC3 signal can be tentatively ascribed to hydroperoxide radicals on CeO_2 surfaces. The interaction of this species with the cerium cations could justify the

deviation of the central component of the *g*-tensor with respect to the free radical. Anyhow, experimental results show that stabilization of the species leading to signal OC3 is not favored on 2D-ceria entities, since no indication of the presence of such radicals on cerium centers are found in CeTi sample.

Assuming the previous assignments, photoactivation of CeO_2 in the presence of oxygen implies the formation of reduced centers that subsequently can transfer electrons to the oxygen molecules. However, as pointed out above, coordination vacancies are also required for the generation of these oxygenated complexes. Coordinative unsaturations are very likely produced by photodesorption of hydroxyl groups. Anyhow, photo-induced production of Ce^{3+}–$V_{\ddot{O}}$ centers in CeO_2 is relatively efficient compared to thermal activation, since outgassing temperatures higher than 373 K are necessary to obtain superoxide species in the dark upon oxygen adsorption at 77 K [17,19]. Although the intensity of the signals produced after irradiation in vacuum is rather weak (Fig. 6a), the subsequent formation of superoxide radicals following oxygen admission (Fig. 6b) reveals that some EPR silent species (i.e. Ce^{3+} centers) are formed already upon RT photoactivation.

3.4. Photocatalytic activity

Photocatalytic activity data in the steady state for the studied catalysts are summarized in Table 2. The rate of toluene PCO of the TiO_2 used in this study is comparable to that obtained for the reference photocatalyst Degussa P25 ($r = 9.0 \times 10^{-10}$ mol s^{-1} m^{-2}) at 343 K [7]. However, a slight reduction in the conversion is observed when utilizing CeTi as catalysts, without any significant change in the selectivity towards benzaldehyde. Catalytic tests carried out in the dark confirmed that the measured activities are fully attributable to photo-induced processes. The PCO rate shows a weak temperature dependence for the two anatase-based catalysts, as expected for a reaction mainly controlled by photoactivated processes. Nevertheless, the production of benzaldehyde increases moderately at 413 K for both TiO_2 and CeTi. Similarities in the performance of these catalysts suggest that PCO take place on both materials according to basically the same mechanism. Previous reports on the toluene photodegradation have proposed that the first step of the oxidation is the attack of $OH^{\bullet}$ species to the organic molecule, yielding a benzyl radical [4]. The photogenerated $OH^{\bullet}$ radicals drive further reactions, as suggested by the detection of phenol traces [4], that eventually can lead to the opening of the aromatic ring. The Ti^{4+}–$OH^{\bullet}$ entities, which are formed by trapping of a hole by a surface hydroxyl, are very difficult to detect directly by EPR because they are extremely reactive [25]. However, some of the photoproduced holes are stabilized as Ti^{4+}–O^{-} radicals (OT2 signals), and their concentration could be an indication of the availability of holes. Consequently, the CeTi catalyst, which displays a reduced concentration of OT2 species, is apparently less prone to trap photogenerated holes than the unmodified TiO_2. In addition, the coverage of the TiO_2 surface by 2D-ceria entities removes OH^{-} groups (Fig. 2), which constitute not only the source of the active $OH^{\bullet}$ radicals but also the adsorption sites for toluene [30]. On the other hand, EPR results for the CeTi sample show that the presence of ceria favors the stabilization of electrons as Ce^{4+}–O_2^{-}. However, the simultaneous photogeneration of Ti^{3+} centers (Fig. 5c) suggests that the electronic transference between the TiO_2 and the CeO_2 occurs to a limited extent. Therefore, the lower PCO rate of CeTi is very likely due to the partial blockage by ceria of the surface centers implied in the trapping of the holes and the adsorption of the organic. Assuming this interpretation and considering the theoretical coverage of CeO_2, the rate for CeTi should be ca. 75% of that of the TiO_2, as found experimentally (Table 2). Consequently, the influence of the Ce^{4+}–O_2 species on the reaction rate, although cannot be totally ruled out, must be rather limited. Finally, the enhancement of the photon harvesting efficiency derived from the red shift of the electronic absorption of CeTi, is not significant under these conditions, because the energy of most of the photons emitted by the UV source (maximum emission at 350 nm) is larger than the bandgap interval of the studied materials.

The photocatalytic performance of CeO_2 shows remarkable differences with respect to the materials based on TiO_2. Thus, this lanthanide oxide displays a PCO rate one order of magnitude lower than the CeTi or TiO_2 materials. However, mineralization of the pollutant is almost complete when CeO_2 is utilized as photocatalyst, and only some traces of benzene are detected at 413 K. The presence of this aromatic compound is not unexpected since it has been previously

Table 2
Reaction rate and selectivity for the PCO of toluene in the steady state for the studied catalysts

Catalyst	Temperature (K)	Reaction rate (mol s^{-1} m^{-2})	Reaction products detected and the corresponding selectivity
TiO_2	343	6.0×10^{-10}	CO_2 (94%), benzaldehyde (6%)
TiO_2	413	6.1×10^{-10}	CO_2 (86%), benzaldehyde (14%)
0.8% CeO_2/TiO_2	343	4.5×10^{-10}	CO_2 (93%), benzaldehyde (7%)
0.8% CeO_2/TiO_2	413	4.7×10^{-10}	CO_2 (87%), benzaldehyde (13%)
CeO_2	343	1.2×10^{-11}	CO_2
CeO_2	413	4.8×10^{-11}	CO_2 with traces of benzene

detected during photodegradation of toluene using undoped anatase as catalyst [4]. On the other hand, an appreciable rise of the PCO rate on the pure cerium oxide is observed with increasing the reaction temperature. In addition, some experiments carried out in the dark at 423 K, using a fixed bed reactor and at lower space velocity, indicate that this material presents some thermal activity for toluene oxidation, as previously reported [31]. These results suggest that the photocatalytic mineralization of toluene can follow a different route on this material. EPR measurements confirm that CeO_2 is photoactivated in the presence of oxygen, giving rise to O_2^- and possibly O_2H radicals. These species might play a role on the photo-oxidation process, but considering the smaller bandgap of CeO_2 compared to the TiO_2-based catalysts (see Fig. 1), a lower redox potential would be expected for the species photogenerated on this lanthanide oxide. As the energy difference between the valence and the conduction band is inversely related to the chemical activity of the charge carriers, holes formed in CeO_2 should be less oxidant than those generated in anatase [9,14]. These considerations could partly account for the lower toluene PCO rate obtained with the CeO_2 catalysts, although other characteristics of this material could also be detrimental for the photoactivity. In any case it is feasible that, oxygen vacancies at the ceria surface, whose generation is favored at high temperature, and/or superoxide species formed on them, could contribute to the photodegradation of toluene. As shown above, centers of the type Ce^{3+}–$V_{Ö}$ can be easily formed by UV irradiation and they are considered to participate in many oxidation reactions [12,31]. Consequently, the main effect of UV light could be to assist the generation of centers for the catalytic degradation of toluene at low temperature. This statement is supported by the observed increment in the PCO rate with the temperature for CeO_2. Changes in the product distribution can also be ascribed to the modification in the reaction route. Regarding this, it is worth noting that the activity of O_2^- species stabilized on cerium centers may significantly modify the selectivity. The influence of the superoxide species on the distribution of products has been confirmed for the photodegradation of quinoline on TiO_2 [32]. In the case of CeTi, dispersed ceria may act in a similar way, but the high PCO rate of the TiO_2 prevents the detection of any additional contribution. In any case, it must be noted that the total mineralization is favored on CeO_2 and this fact may have a practical relevance for preventing the formation of noxious partially oxidized products, if higher PCO rates can be achieved.

4. Conclusions

TiO_2, CeO_2/TiO_2 and CeO_2 materials are shown to present activity for toluene PCO, although the maximum degradation rate corresponds to the pure anatase sample. In the case of the CeO_2/TiO_2 catalyst, EPR results indicate that photoactivation occurs on both components, and some results suggest a limited charge transfer between both components. Experimental results indicate that the main effect of ceria incorporation (in the form of highly dispersed two-dimensional entities) to the titania sample is the partial blockage of the surface sites available for toluene photodegradation. In the case of CeO_2, mineralization of toluene is almost complete, although the oxidation rate is one order of magnitude lower than those of the TiO_2-based materials. This behavior, along with the temperature dependence of the activity, indicates that photo-oxidation takes place according to a different mechanism on CeO_2. The EPR study of the CeO_2 sample shows that UV illumination in the presence of oxygen induces the formation of O_2^- and other radicals, which are derived from trapping of photogenerated electrons. These species may play a role in the photodegradation process, although the lower width of the bandgap interval implies a lower oxidative potential of the holes photoproduced on CeO_2 compared to those formed on anatase. In these conditions, it is proposed that the main effect of UV photoactivation of CeO_2 could be to favor the formation of surface oxygen vacancies.

Acknowledgements

J.M.C. want to thank C.A.M. for the award of a postdoctoral grant. We acknowledge Mr. F. Sánchez Constenla for carrying out some of the EPR measurements.

References

[1] Hester, R.M. Harrison (Eds.), Volatile Organic Compounds in the Atmosphere, The Royal Society of Chemistry, Cambridge, 1995.
[2] J. Peral, D. Ollis, J. Catal. 136 (1992) 554.
[3] M.R. Hoffman, S.T. Martin, W. Choi, D.W. Bahnemann, Chem. Rev. 95 (1995) 69;
A. Linsebigler, G. Lu, J.T. Yates, Chem. Rev. 95 (1995) 735.
[4] V. Augugliaro, S. Coluccia, V. Loddo, L. Marchese, G. Martra, L. Palmisano, M. Schiavello, Appl. Catal. B 15 (1999) 20.
[5] R.M. Alberici, W.F. Jardim, Appl. Catal. B 55 (1995) 14.
[6] A.J. Maira, K.L. Yeung, C.Y. Lee, P.L. Yue, C.K. Chan, J. Catal. 192 (2000) 185.
[7] A.J. Maira, K.L. Yeung, J. Soria, J.M. Coronado, C. Belver, C.Y. Lee, V. Augugliario, Appl. Catal. B 29 (2001) 327.
[8] X. Fu, W.A. Zeltner, M. Anderson, Appl. Catal. B 209 (1995) 6.
[9] J. Lin, J.C. Yu, D. Lo, S.K. Lam, J. Catal. 368 (1999) 183.
[10] M. Anpo, Stud. Surf. Sci. Catal. 157 (2000) 130.
[11] H. Tada, A. Hattori, Y. Tokihisa, K. Imai, N. Tohge, S. Ito, J. Phys. Chem. B 104 (2000) 4586.
[12] A. Trovarelli, Catal Rev. Sci. Eng. 38 (1996) 439.
[13] G.R. Bamwenda, K. Sayama, H. Arakawa, Chem. Lett. 30 (1996) 157.
[14] J. Lin, J.C. Yu, J. Photochem. Photobiol. A 63 (1998) 116.
[15] G.R. Wagner, J. Murphy, Phys. Rev. B 6 (1972) 1638.
[16] A. Bensalem, J.C. Muller, F. Bozon-Verduraz, J. Chem. Soc., Faraday Trans. 153 (1992) 88.
[17] A. Bensalem, F. Bozon-Verduraz, M. Delamar, G. Bugli, Appl. Catal. A 81 (1995) 121.
[18] A. Martínez-Arias, M. Fernández-García, L.N. Salamanca, R.X. Valenzuela, J.C. Conesa, J. Soria, J. Phys. Chem. B 104 (2000) 4035.

[19] C. Morterra, J. Chem. Soc., Faraday Trans. 84 (1988) 1617.
[20] A. Martínez-Arias, J.M. Coronado, J.C. Conesa, J. Soria, in R. Sáez-Puche, P. Caro (Eds.), Rare Earths, Complutense Editorial, Madrid, 1997, p. 299 (Chapter 13).
[21] K. Kholer, C.W. Schläpfer, A. Von Zelewsky, J. Nickl, J. Engweiler, A. Baiker, J. Catal. 143 (1993) 201.
[22] M. Che, J.F.J. Kibblewhite, A.J. Tench, M. Dufaux, C. Naccache, J. Chem. Soc., Faraday Trans. I 69 (1973) 857.
[23] C. Naccache, P. Meriadeau, M. Che, A.J. Tench, J. Chem. Soc., Faraday Trans. I 67 (1971) 506.
[24] R.F. Howe, M. Gräztel, J. Phys. Chem. 89 (1985) 4495; R.F. Howe, M. Gräztel, J. Phys. Chem. 91 (1987) 3906.
[25] O.I. Micic, Y. Zhang, K.R. Cromack, A.D. Trifunac, M.C. Thurnauer, J. Phys. Chem. 97 (1993) 7277.
[26] Y. Nakaoka, Y. Nosaka, J. Photochem. Photobiol. A 110 (1997) 299.
[27] M. Anpo, Y. Kubokawa, T. Fujii, S. Suzuki, J. Phys. Chem. 88 (1984) 2572.
[28] M. Che, A.J. Tench, Adv. Catal. 1 (1983) 132.
[29] D.C. McCain, W.E. Palke, J. Mag. Resonance 20 (1975) 52.
[30] A.J. Maira, J.M. Coronado, V. Augugliario, K.L. Yeung, J.C. Conesa, J. Soria, J. Catal. 202 (2001) 413.
[31] Kuang, K. Fan, K. Chen, Y. Chen, J. Catal. 186 (1999) 310.
[32] J.G. Schwitzgebel, H. Ekerdt, H. Gerischer, A. Heller, J. Phys. Chem. B 99 (1995) 5633.